Resolving Dye Embedment in MOF-5: Multimodal Evidence for Perylene-Based Guest Encapsulation

Fabian L. Schüler, Armin Penz, Marko Panic, Julia Larcher, Jakob Gamper, Svetlana Miliutina, Sofiia Prykhodska, Konstantin Schutjajew, Alexander Knebel, Markus Suta, Thomas S. Hofer, Heidi A. Reichl

ADVANCED OPTICAL MATERIALS
www.advopticalmat.de

Resolving Dye Embedment in MOF-5: Multimodal Evidence for Perylene-Based Guest Encapsulation

Fabian L. Schüler, Armin Penz, Marko Panic, Julia Larcher, Jakob Gamper, Svetlana Miliutina, Sofiia Prykhodska, Konstantin Schutjajew, Alexander Knebel, Markus Suta, Thomas S. Hofer,* and Heidi A. Reichl**

The interplay between two single components within a hybrid system plays a particular role for the formation of new functional materials with specific properties. In this respect, photoactive metal-organic frameworks (MOFs) with a non-covalently bonded incorporated photochromic or luminescent guest are intensively studied due to the beneficial contribution of the MOF scaffold on the switching properties and luminescence brightness. However, a crucial point remains the unambiguous proof of dye embedment as non-covalently attached guest molecule versus dye adsorption on the MOF surface, which cannot be resolved utilizing one specific analysis method. This work illustrates the powerful combination of Powder X-ray diffraction (PXRD), infrared (IR) spectroscopy and N_2 physisorption measurements with advanced photoluminescence studies (steady–state and time-resolved) to monitor the explicit incorporation of perylene derivatives into porous MOF-5. These experimental findings are supported by DFTB3 molecular dynamics (MD) simulations, which show that dyes preferentially occupy large pores, form stable dimers or oligomers, and interact mainly with the MOF's organic linkers.

1. Introduction

MOFs have been an intensively studied class of porous materials over the last decades. MOFs consist of inorganic and organic parts forming 2D or 3D networks with potential voids.[1] The decisive advantage of MOFs over purely inorganic zeolites or even polymers is that they can also be systematically modified according to the principles of crystal engineering[2] by altering their organic linkers or metal nodes. This results in a virtually infinite number of possible framework topologies and properties, which are also interesting in terms of technologically relevant applications such as hydrogen purification,[3] gas storage and separation,[4] photocatalytic solar fuel production,[5] waste water treatment,[6] electrochemical CO_2 reduction,[7] cancer and bacteria inhibition,[8] electrochemical sensors,[9] as cathodes in lithium-ion batteries,[10] or as drug delivery systems.[11] Additionally, they find use as nano-vessel for photoactive molecules, which are non-covalently attached to the MOF scaffold.[12] A central point of discussion remains the unambiguous proof of successful embedment of a (luminescent) dye into the pores instead of the simple attachment to the surface of the MOF. In various studies, PXRD has been utilized to trace the embedment via modulation in MOF reflection intensities due to a change in electron density upon loading, while the absence of additional Bragg reflections indicates the absence of non-embedded crystalline guest molecules.[13–21] X-ray photoelectron spectroscopy (XPS) can serve as a supplementing method, as the embedded guest experiences various electronic

F. L. Schüler, A. Penz, M. Panic, J. Larcher, J. Gamper, T. S. Hofer, H. A. Reichl
Institute of General, Inorganic and Theoretical Chemistry
Universität Innsbruck
Innrain 80–82, Innsbruck A-6020, Austria
E-mail: t.hofer@uibk.ac.at; heidi.schwartz@uibk.ac.at

S. Miliutina, A. Knebel
Otto Schott Institute of Materials Research, Center for Energy and Environmental Chemistry II
Friedrich Schiller University Jena
Lessingstraße 12–14, 07743 Jena, Germany

The ORCID identification number(s) for the author(s) of this article can be found under https://doi.org/10.1002/adom.202501573

DOI: 10.1002/adom.202501573

S. Prykhodska, K. Schutjajew
Institute for Technical Chemistry and Environmental Chemistry
Friedrich Schiller University Jena
Philosophenweg 7a, 07743 Jena, Germany

K. Schutjajew
Helmholtz Institute for Polymers in Energy Applications Jena (HIPOLE Jena)
Lessingstraße 12–14, 07743 Jena, Germany

A. Knebel
Center for Energy and Environmental Chemistry I
Friedrich Schiller University Jena
Philosophenweg 7a, 07743 Jena, Germany

M. Suta
Inorganic Photoactive Materials
Heinrich Heine University Düsseldorf
Universitätsstraße 1, D-40225 Düsseldorf, Germany
E-mail: markus.suta@hhu.de

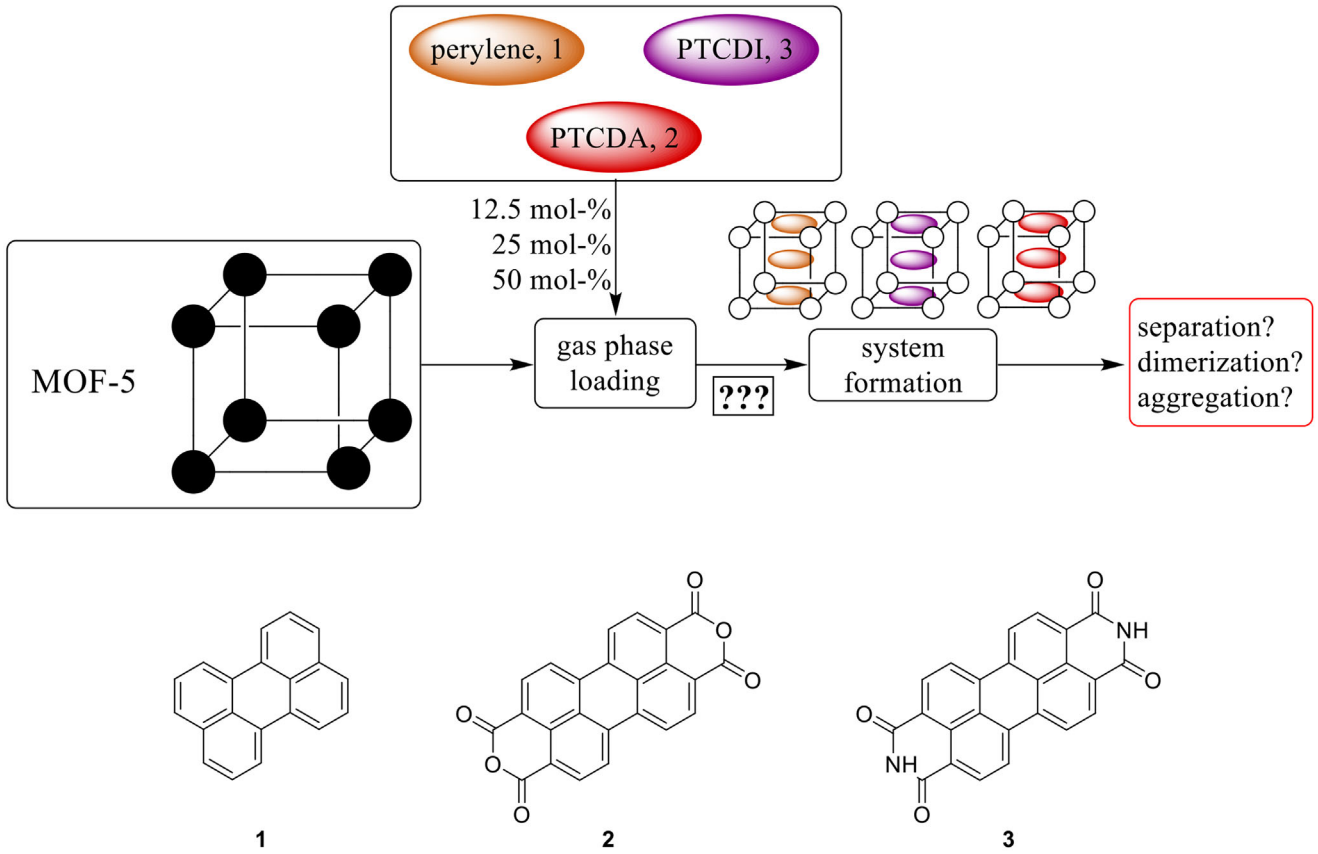

Figure 1. Top: General workflow for the formation of dye@MOF-5 systems; Bottom: Molecular structures of perylene (1), 3,4,9,10-perylenetetradicarboxylicacid dianhydride (PTCDA, 2), and 3,4,9,10-perylenetetracaboxylic diimide (PTCDI, 3).

contributions from the surrounding MOF pore and thus, the XPS signals are broadened. [17] Both PXRD and XPS, however, can only partially resolve potentially present amorphous portions.

In the context of organic fluorophores as non-covalently attached guests, not only MOF dependent changes (via modulation of reflection intensities in the PXRD), but also guest dependent changes can be monitored utilizing spectroscopical methods. In general, MOFs can enhance the luminescent performance of most fluorophores by: 1) reducing the ACQ[22] effect, which allows many guests that show luminescence only in solution to exhibit luminescence in the solid state, and 2) creating a caging effect that decreases nonradiative relaxation, thereby increasing the total decay time (τ) and luminescence quantum yield (Φ) of the guest entities. By utilizing thermally and water-stable MOFs, these can act as protective matrix and with that, improve the stability of the incorporated dye.[23] Within the last years, several organic fluorophores have been embedded into MOFs, which range from coumarin derivatives,[24] flavin derivatives,[25] thioindigo,[20] rhodamine,[26] solvent green 7[27] to fluorescein.[28] Moreover, a plethora of perylene-based MOFs with the perylene dye being part of the linker backbone has been reported.[29–35] However, to date, only few examples of a perylene dye being embedded as non-covalently attached guest molecule were studied to the best of our knowledge.[36–40] Perylene and its derivatives are of special interest, as their optical characteristics rank them among the most attractive hydrocarbons for dyes and pigments: they show a high quantum yield, strong absorption in the UV/Vis range and, in addition, almost no photobleaching.[41]

The advantages of utilizing perylenes in solid-state applications can be leveraged by incorporating them into porous MOFs. Within this work, the optical characteristics of three perylene derivatives (see **Figure 1**) in varying concentrations were studied inside MOF-5.[42] MOF-5, often referred to as the "drosophila" of the MOF compound class, served as a non-emissive and colorless host framework with a suitable pore size and entrance window – not too large, but not too small. The workflow is depicted in the following Figure 1.

Based on that concept, usage of dyes that are prone to the formation of excimers with red-shifted emission upon increase of the dye concentration are an excellent scaffold to investigate the loading of MOF-5 in more depth. For that purpose, we used a combination of IR and luminescence spectroscopy next to the conventional characterization methods such as PXRD and N_2 physisorption measurements. While the latter methods dominantly characterize the reaction of the surrounding host compound, spectroscopic methods can also reveal local phenomena around the guest molecules.

To supplement the experimental investigations of the guest@MOF-5 hybrid systems, host-guest interactions were studied at the molecular scale by utilizing MD simulations at quantum chemical level of theory, employing a self-consistent

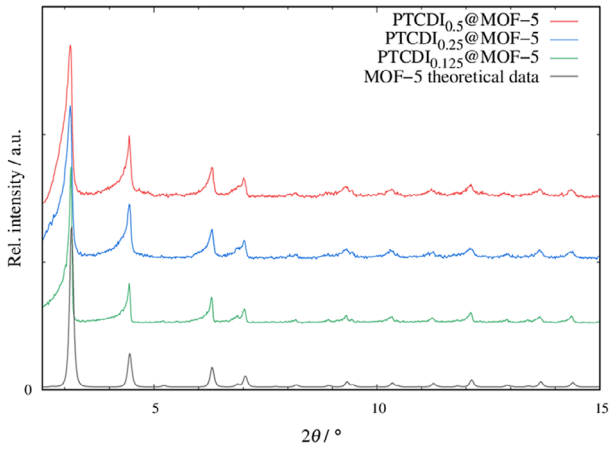

Figure 2. PXRD patterns of $PTCDI_{0.125}$@MOF-5 (green line), $PTCDI_{0.25}$@MOF-5 (blue line), and $PTCDI_{0.5}$@MOF-5 (red line) in comparison to the theoretical data of non-loaded MOF-5. The diffraction patterns were measured at 298 K (Stoe Stadi P, $\lambda = 0.7093$ Å). An offset along y was applied for better clarity.

charge density functional tight binding approach of third order (DFTB3). [20,43,44]

2. Results and Discussion

Dye embedment of perylene, PTCDI as well as PTCDA has been performed via a gas phase loading process to exclude any impact of additional solvent molecules. The successful embedding was monitored via four different methods: PXRD measurements, IR spectroscopy, N_2 physisorption measurements, and luminescence spectroscopy. Additional insights about the host-guest interactions were gained on the molecular scale by utilizing MD simulations at quantum chemical level of theory employing a self-consistent charge density functional tight binding approach of third order (DFTB3).

PXRD is a suitable method to trace dye embedment as the embedding is tractable based on intensity modulations of the Bragg reflections, while additional reflections compared to the non-loaded MOF indicate presence of free crystalline dye molecules. The diffraction patterns of $PTCDI_x$@MOF-5, $perylene_x$@MOF-5 and $PTCDA_x$@MOF-5 ($x = 0.125$, 0.25, or 0.5) are depicted in **Figure 2** (PTCDIx@MOF-5 systems) as well as Figures S1–S3 (Supporting Information), including the corresponding patterns of the respective pristine perylene derivative.

All PXRD patterns of the investigated PTCDI-loaded MOF-5 samples showed no additional reflections and clearly demonstrate the successful formation of the PTCDI@MOF-5 systems (see Figure 2 and Figure S1, Supporting Information). This is also true for other perylene derivatives except $PTCDA_{0.25}$@MOF-5 and $PTCDA_{0.5}$@MOF-5. Here, additional reflections of segregated dye appear at $\approx 2\theta = 5.5°$, which belong to non-embedded crystalline dye (see orange line, Figure S3, Supporting Information). Although heating processes exceeding more than two weeks were applied, these dye-related reflections remained unchanged, pointing to a strong surface adsorption of the PTCDA molecules on MOF-5. Notably, for $perylene_x$@MOF-5 materials, the crystallinity of the systems decreases with higher loading levels (see Figure S2, Supporting Information). This is assumed to be result of strong host-guest interactions, which become especially apparent for these systems. Taking a closer look at the diffraction patterns with PTCDI and PTCDA as guest molecules, there also is a slight decrease in crystallinity when increasing the loading level from 0.125 to 0.25 and 0.5. However, this decrease is not as profound as it is for perylene, which points to a guest size effect. It is not possible to exclude potential amorphous deposits on the MOF surface that cannot be readily characterized by PXRD.

To gain more insights into explicit pore loading of MOF-5 by the added dyes, IR spectroscopy, N_2 physisorption measurements, and luminescence spectroscopy were applied. In the range of 1600–100 cm^{-1}, differences between solid perylene-based dyes and incorporated dyes into MOF-5 are observable (see **Figure 3**). In particular, the signal at 1279 cm^{-1} typical for the aggregated dyes is a strong indication that aggregation is limited upon incorporation into MOF-5. Zhanpeisov et al.[45] reported bands of the perylene core that vanish, when perylene derivatives are present as monomer or dimer as an effect of intermolecular interactions. Similar results were published by Ding et al.[46] The corresponding band at 1279 cm^{-1} is present in pure perylene, but not in any dilute systems (see Figure 3, top, left). It can be concluded that the aggregation of the perylene dyes in all regarded systems is limited to the formation of a dimer. $PTCDI_x$@MOF-5 and $PTCDA_x$@MOF-5 systems show a similar behavior as $perylene_x$@MOF-5 regarding the intermolecular interactions and the maintenance of the single components spectral signature (see Figure 3, top, right and bottom). A summary of all assigned bands related to $PTCDI_x$@MOF-5 systems is compiled in Table S2 (Supporting Information), while that for $PTCDA_x$@MOF-5 is summarized in Table S3 (Supporting Information). Analogously to the perylene dye, bands at 1276 cm^{-1} or 1265 indicate the presence of PTCDI or PTCDA aggregates greater than monomers or dimers, respectively.[45,46] For $PTCDI_x$@MOF-5, they are present in all systems except $PTCDI_{0.125}$@MOF-5. Thus, at 25 mol% and 50 mol%, PTCDI associates into oligomeric aggregates larger than simple dimers. For $PTCDA_x$@MOF-5, this band is not found in any system. Similar to perylene, PTCDA maximally aggregates as a dimer within the MOF-5 scaffold. Via IRspectroscopy, the effect of dye intercalation into the hosting MOF-5 as well as potential dye aggregation was monitored (Figure 3).

N_2 physisorption measurements at 77 K of MOF-5 and the hybrid systems are essential for gaining a comprehensive understanding of the changes in porosity induced by guest loading at varying molar fractions x.[47,48] The results of these measurements are shown in **Figure 4**. The pristine MOF-5 exhibits a Type I(a) isotherm, corresponding to a predominantly microporous structure.[49] It also shows a H_2-type hysteresis, reflecting mesoporous cavities with narrow openings within the mainly microporous framework. This behavior could be related to defects in the framework or to gaps between particles.[50]. A pore size distribution obtained from the non-local density functional theory (NLDFT) (Figure S5, Supporting Information), assuming cylindrical pores and assuming silica/zeolite surfaces, confirms a predominantly microporous structure with small fractions of mesopores smaller than 10 nm. The surface area obtained by Brunauer Emmett Teller (BET) method, SSA_{BET}, is 1100 $m^2\ g^{-1}$

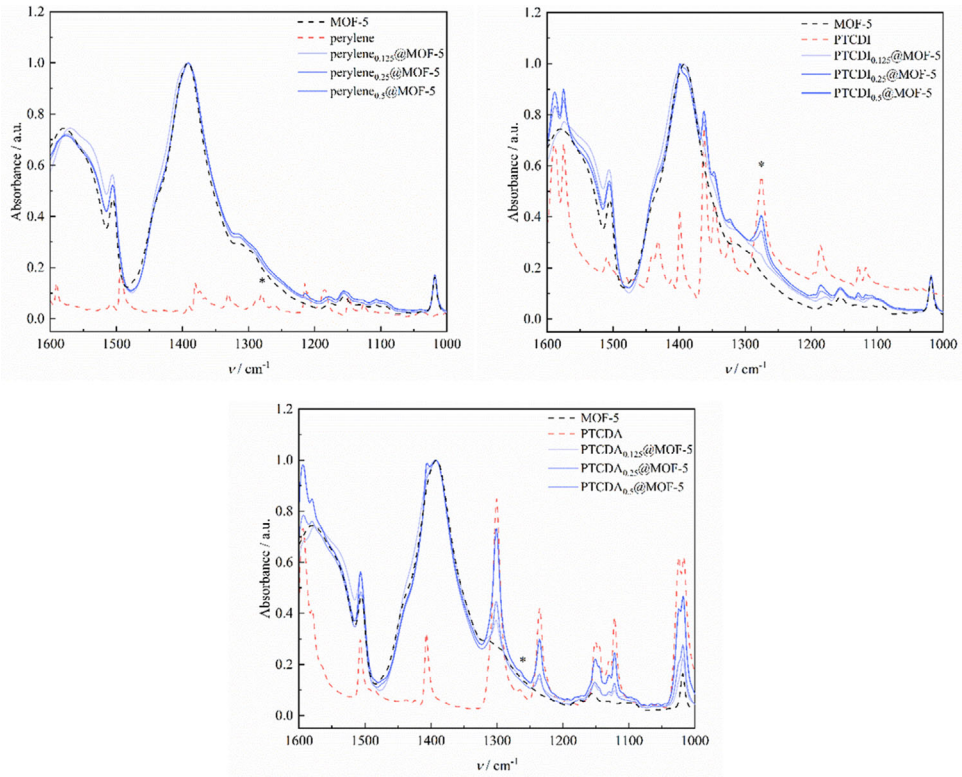

Figure 3. Top: IR spectra of perylene$_{0.125}$@MOF-5, perylene$_{0.25}$@MOF-5, and perylene$_{0.5}$@MOF-5; center: IR spectra of PTCDI$_{0.125}$@MOF-5, PTCDI$_{0.25}$@MOF-5, and PTCDI$_{0.5}$@MOF-5; bottom: IR spectra of PTCDA$_{0.125}$@MOF-5, PTCDA$_{0.25}$@MOF-5, and PTCDA$_{0.5}$@MOF-5. All spectra are compared to the non-loaded MOF-5 (dashed black line) and the respective pure solid dye (dashed orange line). The asterisks mark the respective aggregate band. Measurements were performed on a KBr pellet at room temperature.

(Table S7, Supporting Information), falling within the characteristic range reported for MOF-5.[51] After loading of perylene, PTCDA, and PTCDI the values of SSA_{BET} and total pore volume, V_{total}, determined under the assumption that the density of the adsorbate within the pores equals the bulk liquid density at the same temperature and pressure,[52] are expectedly lower than those for pristine MOF-5, due to introduction of guest molecules into the MOF framework (Tables S7–S9, Supporting Information). The system perylene$_x$@MOF-5 demonstrates a gradual reduction in SSA_{BET} as well as V_{total} upon the progressive incorporation of guest molecules. (Table S7, Supporting Information). PTCDA$_x$@MOF-5 hybrids also show the same trend in V_{total} values, but SSA_{BET} for the loading of $x = 0.125$ deviates (Table S8, Supporting Information). This deviation could be related to the low mass of the sample analyzed, which introduces uncertainties in the BET fitting. For PTCDI$_x$@MOF-5 at $x = 0.125$ and $x = 0.25$, the value of SSA_{BET} is decreasing with increasing loading. However, for PTCDI$_{0.25}$@MOF-5 there is a slight increase

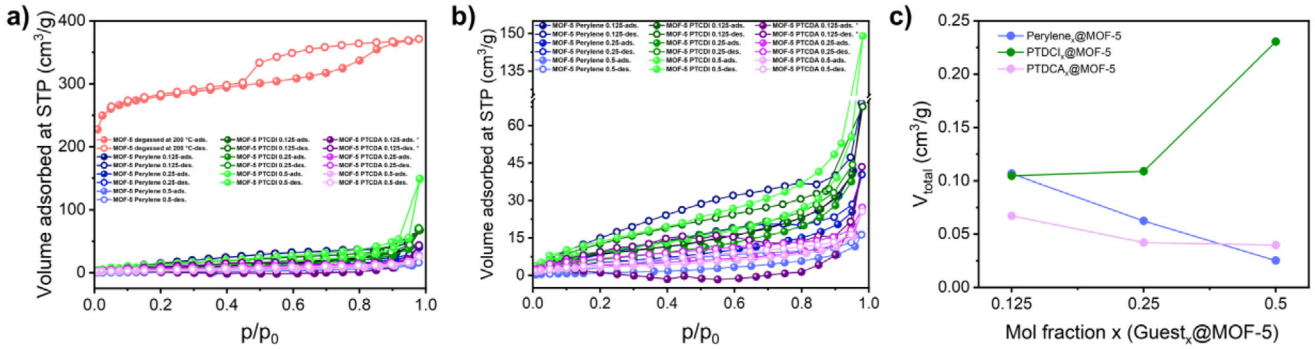

Figure 4. N_2 physisorption results. The asterisk at PTCDI$_{0.125}$@MOF-5 marks a data point that has a low accuracy because of low sample mass. a) N_2 volume adsorbed on samples including the pristine MOF-5 as well as perylene$_x$@MOF-5, PTCDA$_x$@MOF-5, and PTCDI$_x$@MOF-5 with $x = 0.125$, 0.25, and 0.5. b) The same image as in a) but with a different y-axis scale for better visibility. c) Total volume over the perylene$_x$@MOF-5, PTCDA$_x$@MOF-5. and PTCDI$_x$@MOF-5 with $x = 0.125$, 0.25, and 0.5 showing a clear trend.

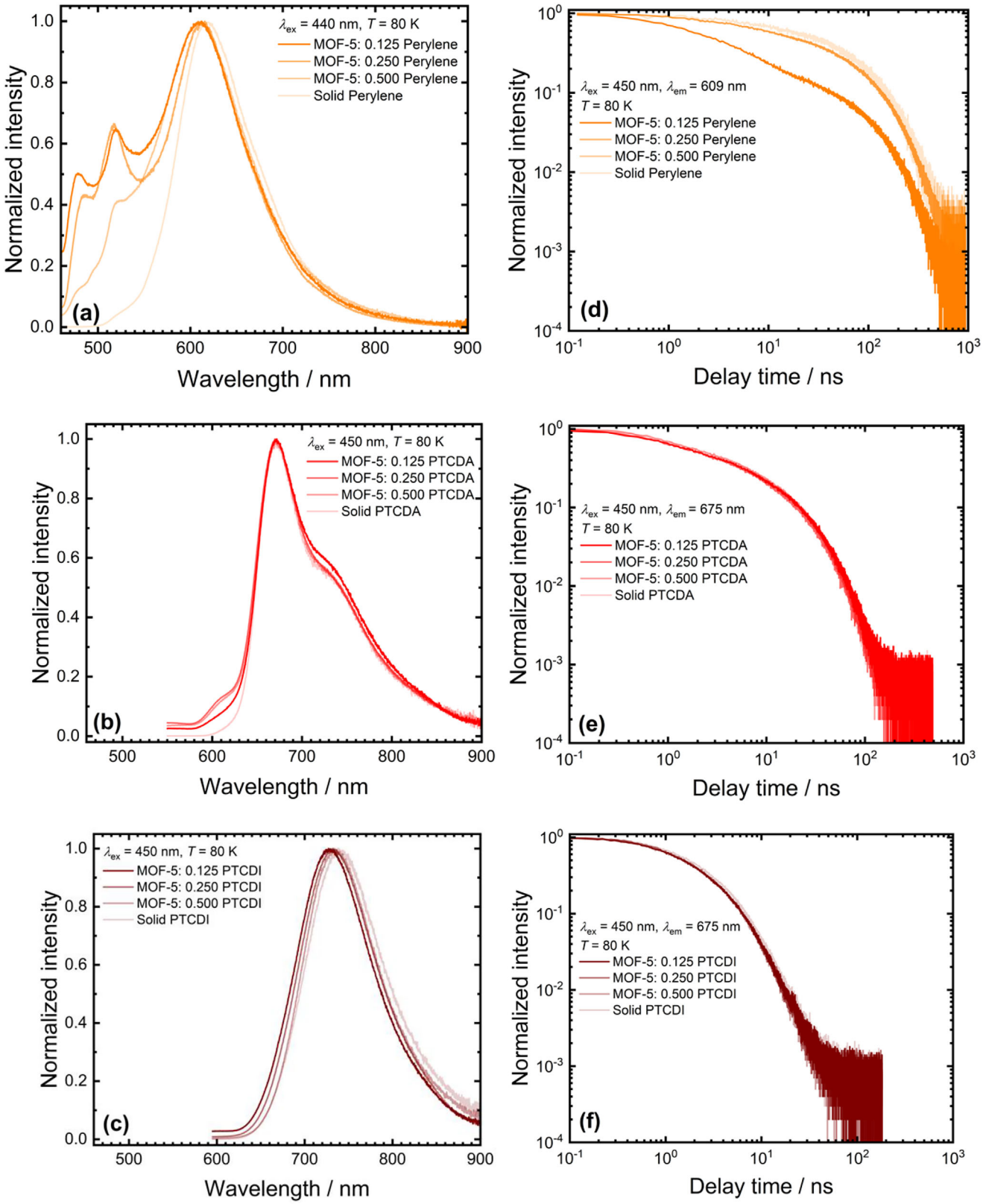

Figure 5. Left panels: Steady–state photoluminescence spectra of a) perylene$_x$@MOF-5, b) PTCDA$_x$@MOF-5, and c) PTCDI$_x$@MOF-5 at $T = 80$ K. Right panels: Luminescent decay traces of the incorporated dyes d) perylene$_x$@MOF-5, e) PTCDA$_x$@MOF-5, and e) PTCDI$_x$@MOF-5 ($x = 0.125, 0.250, 0.500, 1.000$) compared to the pure dyes at $T = 80$ K.

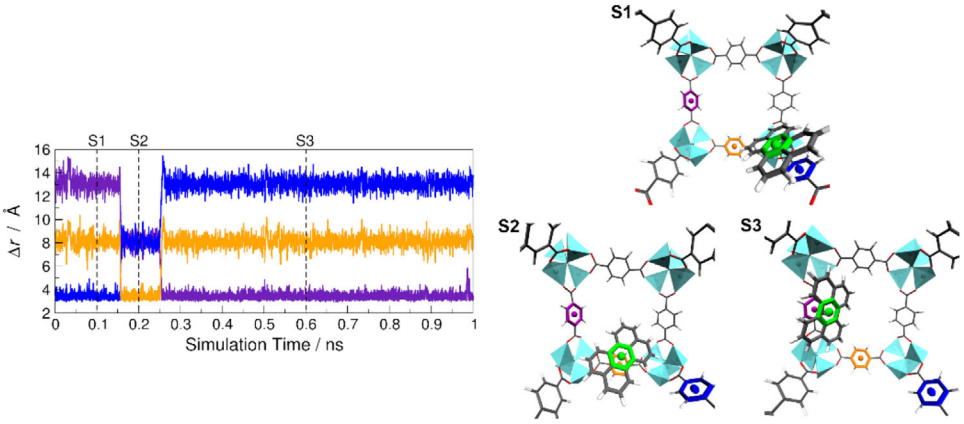

Figure 6. Time series of the centroid-centroid distance Δr considering the central ring of perylene (green) to the aromatic ring of different linker molecules of MOF-5 (blue, orange, purple). Initially, the guest was located in a small pore and migrated into a large pore already in the equilibration period (not shown). Snapshots are taken at 0.1 ns (S1), 0.2 ns (S2), and 0.6 ns (S3) to highlight key configurations.

in V_{total}. Furthermore, at the highest loading (PTCDI$_{0.5}$@MOF-5), both SSA_{BET} and V_{total} values show an increase. This observation is in accordance with the IR data presented in Figure 3, from which guest-guest interaction and aggregation is observed. For PTCDA and perylene, a non-ordered self-assembly is often observable. Furthermore, it is observed that self-assembly of PTDCI could be a possible explanation for this behavior.[53]

Figure 5 depicts the representative steady-state and time-resolved photoluminescence properties of the perylene$_x$@MOF-5, PTCDA$_x$@MOF-5, and PTCDI$_x$@MOF-5 system compared to the pure powdered perylene-based dyes at $T = 80$ K. No photobleaching effects were observed throughout the experiments, which are a known problem for perylene-based dyes at high irradiance in the order of kW cm^{-2}.[54] We ascribe the photostability of the composites in our experiments to the much lower irradiance of the used Xe arc lamp (see Experimental Part in the Supporting Information for more details). The emission of the perylene- and PTCDI-loaded system shows a slight redshift upon increasing loading of MOF-5 and in the solid dyes. The luminescence spectra of the PTCDA-loaded system are insignificantly affected by the loading amount. In addition, time-resolved luminescence was probed as aggregation effects often have an impact on decay times. For PTCDA and PTCDI, the fluorescence decay times in the order of 10 ns (PTCDA) or 6 ns (PTCDI) are not significantly affected and agree within all investigated samples and reports on perylene diimide dyes in solution.[55] However, there is a general elongation of the average decay time of the perylene-loaded MOF systems upon increasing loading amount, which may be ascribed to gradual aggregation effects. This is in line with the observation from the luminescence spectra that show an intensity decrease of the narrower, blue-shifted emission bands compared to the most dominant emission band at 610 nm. Overall, these findings imply that aggregation of the perylene dyes is inhibited upon contact with MOF-5 (see Figure 5a,d). While the results from luminescence spectroscopy themselves are not unambiguous proof that the dye molecules are really incorporated into the pores, the combination with the results from PXRD, IR spectroscopy and N_2 physisorption measurements do strongly favor the conclusion of incorporation of the perylene dyes into the MOF pores. It is noteworthy that absolute quantum yield measurements are not helpful in this regard as the absolute quantum yield does also depend on factors such as sample quality, defect concentration or crystallinity and thus, may not readily serve as a robust, comparable measure among the various powdered samples. It can be, however, deduced that the internal quantum yield of the emitters must be similar based on the similar decay times.

In addition to the experimental investigations, 3rd order density functional tight binding molecular dynamics (DFTB3 MD) simulations of perylene$_x$@MOF-5, PTCDA$_x$@MOF-5, and PTCDI$_x$@MOF-5 ($x = 1, 2$) systems have been carried out on the nanosecond scale to provide insight into the respective host-guest and guest-guest interactions guiding the optical properties. The migration of the guest molecules inside MOF-5 was traced using pair distances based on the centroids calculated for the aromatic moieties of the BDC^{2-} linkers and the guests as exemplarily shown in case of perylene@MOF-5 in the following **Figure 6**.

Similar centroid-centroid distance analyses of all other systems investigated are provided in Figures S6 and S7 (Supporting Information). Based on DFTB3 MD simulations at ambient conditions the guest molecules adopt the thermodynamically most favorable interaction motif, which is of particular advantage over simple structure optimizations that only collapse to the nearest local minimum structure. **Figure 7** provides an overview of the most stable interaction motifs identified via DFTB3 MD simulations of perylene, PTCDA and PTCDI monomers and dimers embedded in MOF-5. From these structures the average interaction energies can be determined providing detailed insight into the host-guest interaction (see also Table S10, Supporting Information).

As expected, perylene displays the weakest host-guest interactions within MOF-5, yielding interaction energies of $U_{int} = -90.6$ and -92.3 kJ mol^{-1} upon embedment of a single molecule in a small and a large pore of MOF-5. PTCDA and PTCDI exhibit notably stronger interactions amounting to -109.9 and -110.1 kJ mol^{-1} (small pore) as well as -111.9 and -116.4 kJ mol^{-1} (large pore), respectively. Increase of the loading of the host to two guest molecules resulted in interaction energies of -195.4, -272.0, and -284.9 kJ mol^{-1}, respectively. These values significantly exceed twice the value for single occupation, indicating pronounced guest-guest interactions. In case of PTCDI, the most stable

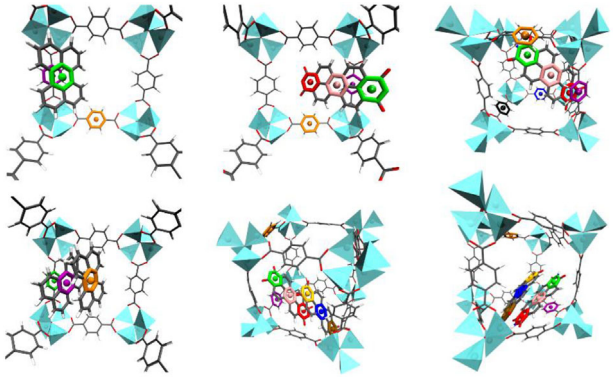

Figure 7. Overview of the most stable interaction motifs between perylene (left), PTCDA (center) and PTCDI (right) in the MOF-5 host considering single (top) and double (bottom) occupation.

motif was only found after heating the system to 350 K followed by cooling to ambient conditions. In order to obtain further insight into the guest-guest interactions, MD simulations of the stacked dimers and trimers were performed in vacuum at 298 K. The respective average interaction energies are listed in Table S10 (Supporting Information). The oligomers of PTCDI in vacuum show a higher energetic stabilization than those of PTCDA, which in turn are more stable than the perylene oligomers. In the case of PTCDA and PTCDI, the energy obtained per monomer decreases from dimer to trimer. This is most likely due to the fact that the displacement of the dimer from its energetically favorable equilibrium distance cannot be compensated for by the additional atomic interactions in the respective trimers. In particular, PTCDI is the only guest molecule that shows stronger binding as a dimer in vacuum than when embedded in the MOF-5 matrix.

As a general trend, perylene, PTCDA and PTCDI prefer occupying a large pore of MOF-5 over a small pore, while exhibiting pronounced guest-guest stacking inside the host matrix at room temperature. The combined results of the interaction energies and analysis of the simulation trajectories lead to the conclusion that the three perylene-based guest molecules establish strong non-covalent binding motifs with the aromatic rings of the linker molecules when introduced into MOF-5. Close interactions between the guest molecule and the inorganic $[Zn_4O]^{6+}$ clusters are avoided in all investigated systems. The strong host-guest interactions are in excellent agreement with the previously described experimental results as well as reports from laser flash photolysis of the PTCDA@MOF-5 system.[31]

3. Conclusion

In conclusion, the successful incorporation of perylene, PTCDI, and PTCDA dyes into the MOF-5 framework via gas phase loading has been convincingly demonstrated through a combination of PXRD, IR, N_2 physisorption measurements and luminescence spectroscopy, complemented by advanced molecular dynamics simulations. PXRD confirmed dye embedment and distinguished between pore loading and potentially present crystalline dye on the surface of the MOF, while IR spectroscopy provided evidence for limited dye aggregation within the MOF pores, mostly restricted to oligomer and dimer formation. Successful embedment and potential aggregation behavior were additionally traced by N_2 physisorption measurements. Luminescence studies further supported the inhibition of dye aggregation upon MOF embedding, as reflected in shifts of selected emission bands and an effect on the average fluorescence decay times. These experimental observations were strongly corroborated by DFTB3 MD simulations, which revealed favorable host-guest and guest-guest interaction motifs, with dyes preferentially occupying large pores and forming energetically stable dimers or oligomers. The simulations also confirmed that guest molecules interact primarily with the organic linkers rather than the metal clusters of MOF-5. Overall, the synergy between experimental and computational approaches provides a comprehensive understanding of the structural and optical behavior of perylene-based dyes within the MOF-5 matrix, laying a solid foundation for the design of advanced photonic or optoelectronic materials based on dye@MOF composites.

4. Experimental Section

Chemicals: Details on the chemicals used can be found in the Supporting Information.

Synthesis of MOF-5 and the guest@MOF Systems: MOF-5 was synthesized following the protocol given in the literature.[56] Perylene, PTCDA and PTCDI molecules were incorporated into MOF-5 via gas phase synthesis at elevated temperatures under reduced pressure. In Tables S1–S3 (Supporting Information), the weighed-in masses and temperatures were listed. The phase purity was confirmed by PXRD.

Powder X-Ray Diffraction: To probe the phase purity of the MOF host as well as the successful incorporation of the perylene derivatives, powder x-ray diffraction (PXRD) was applied. Measurements were carried out with a Stoe Stadi P diffractometer (Stoe, Darmstadt, Germany) in transmission geometry with Mo-$K_{\alpha 1}$ radiation (λ = 70.93 pm) utilizing a focusing Ge(111) primary beam monochromator and a Mythen 2 DCS4 detector. Data was collected in the 2θ range of 2.0–40.4° with a step size of 0.015°. For each measurement, the respective sample was sealed in a glass capillary under argon atmosphere to prevent absorption of humidity. All measurements were carried out at room temperature.

Infrared Spectroscopy: Infrared (IR) spectroscopic measurements were carried out on a Bruker Alpha II FT-IR-Spectrometer under argon atmosphere. For this, half of a tip of a spatula of the sample was thoroughly ground with two spatulas of KBr and pressed to a thin transparent KBr pellet with a set pressure of ≈2 tons for 30 min. Scans were done in the range of 360 to 4000 cm^{-1} with a resolution of 2 cm^{-1} and 90 scans per sample. The background (a pure KBr pellet) was measured with the same instrument settings as the sample and subtracted subsequently after each measurement. All measurements were performed at room temperature. Evaluation of data was performed with the program OPUS version 8.2 build 8, 2, 28 (20 190 310) Copyright© Bruker Optic GmbH.

Luminescence Spectroscopy: Steady–state excitation and emission spectra were acquired on a FLS1000 spectrometer from Edinburgh Instruments equipped with a 450 W Xe arc lamp, double Czerny-Turner grating monochromators in both the excitation and emission compartment (focal length 2 × 325 mm), and a thermoelectrically cooled (−20 °C) Hamamatsu PMT-980 photomultiplier tube as a detector. All spectra were corrected with respect to the grating efficiency, the excitation spectra were additionally corrected with respect to the lamp intensity, while emission spectra were additionally corrected with respect to the wavelength-dependent detector sensitivity. Time-resolved luminescence in the ns time range was measured with a pulsed mode-locked laser diode from Edinburgh Instrument (λ_{ex} = 450 nm, temporal pulse width $\Delta\tau \approx$ 75 ps, common repetition rates between 2 MHz and 20 MHz), while the signal was detected with

time-correlated single photon counting (TCSPC) and binned over maximum 8192 available channels. The sample temperature was controlled with a fiber-coupled Linkam THMS600 temperature stage (accuracy ± 0.1 K).

Physisorption: Volumetric N_2 physisorption was performed on a Quantachrome Quadrasorb at 77 K. The loaded samples were degassed under vacuum and RT for 20 h to not desorb the luminescent guest molecules. Neat MOF-5 was degassed at 473.15 K for 20 h to obtain comparable results to literature data. Specific internal surface area was determined using Brunauer-Emmett-Teller (BET) theory $SSA_{BET,N2}$, in the relative pressure (p/p_0) region of ≈0.009 – 0.251 at the N_2-physisorption isotherms. By using local density functional theory (NLDFT), pore size distributions could be determined. To obtain total pore volumes, the Gervich rule was applied, assuming that the desorbed vapor of the gas in the pores is equal to their bulk liquid density at the same T and p. For all data processing, silica/zeolite surface and approximately cylindrical pores were assumed.[52,57]

DFTB Calculation Framework: Quantum chemical energy and force calculations were performed via the DFTB3 method as implemented in the DFTB+ program package[58] utilizing the 3obwp set of parameters[59–61] and the DFT-D3 dispersion correction.[62] An exponent of 4.0 inside the damping factor was chosen to ensure correct interatomic short-range interactions involving hydrogen atoms. Recent work has shown that due to the relatively large size of the MOF-5 unit cell, Γ-point sampling of the Brillouin zone is sufficient to treat interactions inside the periodic system.[21] The convergence criterion for the charge error in every SCC cycle was set to 10^{-4} a. u., corresponding to an error in the energy of less than 10^{-6} Hartree.

Molecular Dynamics Simulation Setup: The DFTB+ package has been interfaced with our in-house developed QM/MM MD simulation program.[63–65] For time integration, the velocity Verlet integrator[66] was utilized. All bonds involving hydrogen atoms have been constrained to their average distance via the RATTLE algorithm[67] to enable an increased time step of 2.0 fs. The Bussi-Donadio-Parrinello thermostat[68] with a relaxation time of 0.1 ps was utilized to maintain a temperature of 298.15 K during the individual simulations. The pressure was set to 1.013 bar by applying the Berendsen manostat[69] with a relaxation time of 10 ps. All simulations were carried out under isotropic conditions. Key configurations observed during the MD simulations are visualized using the program Visual Molecular Dynamics (VMD).[70] The various guest@MOF-5 hybrid systems were generated by introducing the three different guest molecules perylene, PTCDA and PTCDI in a random manner into the equilibrated host matrix, while ensuring a minimum host-guest distance of 1.7 Å. One guest at a time was inserted into either a small or a large pore of MOF-5. Furthermore, simulation setups with two identical guests per unit cell were constructed by placing one guest in a small and the other in a large pore (referred to as "2 Pore Setup" in the following). To enable a temperature dependent comparison in the case of PTCDI@MOF-5 two additional runs were conducted by heating the initial system with two guests per unit cell to 350 K and cooling the resulting configuration back down to 298.15 K. Thus, a total of eleven initial starting structures were prepared. Each system was re-equilibrated for 10 000 MD steps (0.02 ns), before the associated configurational space was sampled for a minimum of 500 000 MD steps (1 ns), resulting in a total DFTB3 MD simulation time of guest@MOF-5 systems exceeding 11 ns during the course of this investigation. The interaction energies of perylene, PTCDA and PTCDI homo dimers and trimers in vacuum were studied by placing the target molecules in a simulation cell of 100 Å edge length. After 1 000 MD steps (2 ps) of initial equilibration, the systems were sampled for a total of 200 000 MD steps (0.4 ns) each.

Supporting Information

Supporting Information is available from the Wiley Online Library or from the author.

Acknowledgements

F.L.S. and A.P. contributed equally to this work. This research was funded in part by the Austrian Science Fund (FWF) grant DOI: 10.55776/I6735. For open access purposes, the author has applied a CC BY public copyright license to any author who accepted manuscript version arising from this submission. J.L., A.P., M.P., T.S.H. and H.A.S. thank the F.W.F. for funding. A.K. and S.M. acknowledge funding through the DFG withing RTG 3014 PhInt – Photo-Polarizable Interfaces and Membranes (Project no. 521747072). Prof. Dr. Martin Oschatz is acknowledged for the physisorption measurements in his group. The computational results of this work have been computed (in part) using the HPC infrastructure LEO5 of the Universität Innsbruck. M.S.x is grateful for a materials cost allowance of the Fonds der Chemischen Industrie e.V. and funding by the "Young College" of the North-Rhine Westphalian Academy of Science, Humanities, and the Arts.

Conflict of Interest

The authors declare no conflict of interest.

Data Availability Statement

The data that support the findings of this study are available from the corresponding author upon reasonable request.

Keywords

host-guest systems, hybrid materials, luminescence, MD simulations, MOFs

Received: May 17, 2025
Revised: September 29, 2025
Published online: October 16, 2025

[1] S. R. Batten, N. R. Champness, X.-M. Chen, J. Garcia-Martinez, S. Kitagawa, L. Öhrström, M. O 'Keeffe, M. P. Suh, J. Reedijk, *Pure Appl. Chem.* **2013**, *85*, 1715.
[2] A. K. Nangia, G. R. Desiraju, *Angew. Chem., Int. Ed.* **2019**, *58*, 4100.
[3] S. Chen, M. Wahiduzzaman, T. Ji, Y. Liu, Y. Li, C. Wang, Y. Sun, G. He, G. Maurin, S. Wang, Y. Liu, *Angew. Chem., Int. Ed.* **2024**, *64*, 202413701.
[4] T. Jia, Y. Gu, F. Li, *J. Environ. Chem. Eng.* **2022**, *10*, 108300.
[5] P. M. Stanley, J. Haimerl, C. Thomas, A. Urstoeger, M. Schuster, N. B. Shustova, A. Casini, B. Rieger, J. Warnan, R. A. Fischer, *Angew. Chem., Int. Ed.* **2021**, *60*, 17854.
[6] F. Yang, M. Du, K. Yin, Z. Qiu, J. Zhao, C. Liu, G. Zhang, Y. Gao, H. Pang, *Small* **2022**, *18*, 2105715.
[7] J. Chen, G. Wang, Y. Dong, J. Ji, L. Li, M. Xue, X. Zhang, H. M. Cheng, *Angew. Chem., Int. Ed.* **2024**, *64*, 202416367.
[8] J. E. Cun, X. Fan, Q. Pan, W. Gao, K. Luo, B. He, Y. Pu, *Adv. Colloid Interface Sci.* **2022**, *305*, 102686.
[9] N. Kajal, V. Singh, R. Gupta, S. Gautam, *Environ. Res.* **2022**, *204*, 112320.
[10] R. C. K. Reddy, X. Lin, A. Zeb, C. Y. Su, *Electrochem. Energy Rev.* **2022**, *5*, 312.
[11] P. Horcajada, C. Serre, M. Vallet-Regí, M. Sebban, F. Taulelle, G. Férey, *Angew. Chem., Int. Ed.* **2006**, *45*, 5974.
[12] G. C. Thaggard, B. K. P. M. Kankanamalage, K. C. Park, J. Lim, M. A. Quetel, M. Naik, N. B. Shustova, *Adv. Mater.* **2024**, 2410067.

[13] D. Hermann, H. Emerich, R. Lepski, D. Schaniel, U. Ruschewitz, *Inorg. Chem.* **2013**, *52*, 2744.
[14] D. Hermann, H. A. Schwartz, M. Werker, D. Schaniel, U. Ruschewitz, *Chem. - Eur. J.* **2019**, *25*, 3606.
[15] H. A. Schwartz, H. Laurenzen, S. Kerschbaumer, M. Werker, S. Olthof, H. Kopacka, H. Huppertz, K. Meerholz, U. Ruschewitz, *Photochem. Photobiol. Sci.* **2020**, *19*, 1730.
[16] H. A. Schwartz, S. Olthof, D. Schaniel, K. Meerholz, U. Ruschewitz, *Inorg. Chem.* **2017**, *56*, 13100.
[17] H. A. Schwartz, M. Werker, C. Tobeck, R. Christoffels, D. Schaniel, S. Olthof, K. Meerholz, H. Kopacka, H. Huppertz, U. Ruschewitz, *ChemPhotoChem* **2020**, *4*, 195.
[18] K. Küssner, R. V. Listyarini, M. Rödl, S. Olthof, K. Meerholz, T. S. Hofer, H. A. Schwartz, *Chem. Mater.* **2023**, *35*, 6953.
[19] C. Eichler, A. Rázková, F. Müller, H. Kopacka, H. Huppertz, T. S. Hofer, H. A. Schwartz, *Chem. Mater.* **2021**, *33*, 3757.
[20] A. Fischereder, M. Rödl, M. Suta, T. S. Hofer, H. A. Schwartz, *J. Phys. Chem. C* **2023**, *127*, 15657.
[21] F. R. S. Purtscher, L. Christanell, M. Schulte, S. Seiwald, M. Rödl, I. Ober, L. K. Maruschka, H. Khoder, H. A. Schwartz, E. E. Bendeif, T. S. Hofer, *J. Phys. Chem. C* **2022**, *127*, 1560.
[22] R. F. Chen, J. R. Knutson, *Anal. Biochem.* **1988**, *172*, 61.
[23] M. Gutiérrez, Y. Zhang, J. C. Tan, *Chem. Rev.* **2022**, *122*, 10438.
[24] Y. Wen, T. Sheng, X. Zhu, C. Zhuo, S. Su, H. Li, S. Hu, Q.-L. Zhu, X. Wu, *Adv. Mater.* **2017**, *29*, 1700778.
[25] D. Püschel, S. Hédé, I. Maisuls, S. P. Höfert, D. Woschko, R. Kühnemuth, S. Felekyan, C. A. M. Seidel, C. Czekelius, O. Weingart, C. A. Strassert, C. Janiak, *Molecules* **2023**, *28*, 28062877.
[26] W. Chen, Y. Zhuang, L. Wang, Y. Lv, J. Liu, T. L. Zhou, R. J. Xie, *ACS Appl. Mater. Interfaces* **2018**, *10*, 18910.
[27] H. R. Fu, X. X. Wu, L. F. Ma, F. Wang, J. Zhang, *ACS Appl. Mater. Interfaces* **2018**, *10*, 18012.
[28] T. Xiong, Y. Zhang, L. Donà, M. Gutiérrez, A. F. Möslein, A. S. Babal, N. Amin, B. Civalleri, J. C. Tan, *ACS Appl. Nano Mater.* **2021**, *4*, 10321.
[29] N. Sikdar, D. Dutta, R. Haldar, T. Ray, A. Hazra, A. J. Bhattacharyya, T. K. Maji, *J. Phys. Chem. C* **2016**, *120*, 13622.
[30] J. M. Wang, L. Y. Yao, W. Huang, Y. Yang, W. Bin Liang, R. Yuan, D. R. Xiao, *ACS Appl. Mater. Interfaces* **2021**, *13*, 44079.
[31] G. Valente, M. Esteve-Rochina, S. P. C. Alves, J. M. G. Martinho, E. Ortí, J. Calbo, F. A. A. Paz, J. Rocha, M. Souto, *Inorg. Chem.* **2023**, *62*, 7834.
[32] A. Adawiah, A. Zulys, I. Fitria, M. Khalil, I. Aziz, M. Khalid, *South African J. Chem. Eng.* **2025**, *53*, 319.
[33] D. Lai, Z. Mu, J. Zuo, J. Zhou, Q. Zhang, K. Chen, L. Bai, H. Liang, *ACS Appl. Nano Mater.* **2023**, *6*, 22416.
[34] C. Wei, M. Lu, J. J. Li, Z. J. Diao, G. Liu, X. Q. Liu, L. B. Sun, *J. Mater. Chem. A* **2024**, *12*, 33142.
[35] I. Romero-Muñiz, J. García-Calvo, C. Romero-Muñiz, D. R. San-Miguel, T. Torres, F. Zamora, G. Bottari, *Adv. Opt. Mater.* **2025**, *13*, 2402127.
[36] R. Ballesteros-Garrido, A. P. Da Costa, P. Atienzar, M. Alvaro, C. Baleizão, H. García, *RSC Adv.* **2016**, *6*, 35191.
[37] X. Zhou, J. Li, L. L. Tan, Q. Li, L. Shang, *J. Mater. Chem. B* **2020**, *8*, 3661.
[38] I. H. Park, A. Dey, K. Sasaki, M. Ohba, S. S. Lee, J. J. Vittal, *IUCrJ* **2020**, *7*, 324.
[39] Y. Cui, R. Song, J. Yu, M. Liu, Z. Wang, C. Wu, Y. Yang, Z. Wang, B. Chen, G. Qian, *Adv. Mater.* **2015**, *27*, 1420.
[40] Q. Q. Xia, X. H. Wang, J. L. Yu, Z. Y. Xue, J. Chai, M. X. Wu, X. Liu, *Dalton Trans.* **2022**, *51*, 9397.
[41] J. T. Markiewicz, F. Wudl, *ACS Appl. Mater. Interfaces* **2015**, *7*, 28063.
[42] H. Li, M. Eddaoudi, M. O'Keeffe, O. M. Yaghi, *Nature* **1999**, *402*, 276.
[43] M. Rödl, A. Reka, M. Panic, A. Fischereder, M. Oberlechner, T. Mairegger, H. Kopacka, H. Huppertz, T. S. Hofer, H. A. Schwartz, *Langmuir* **2022**, *38*, 4295.
[44] R. V. Listyarini, J. Gamper, T. S. Hofer, *J. Phys. Chem. B* **2023**, *127*, 9378.
[45] N. U. Zhanpeisov, S. Nishio, H. Fukumura, *Int. J. Quantum Chem.* **2005**, *105*, 368.
[46] L. Ding, P. Schulz, A. Farahzadi, K. V. Shportko, M. Wuttig, *J. Chem. Phys.* **2012**, *136*, 054503.
[47] M. Shiri, M. Hosseinzadeh, S. Shiri, S. Javanshir, *Sci. Rep.* **2024**, *14*, 20206.
[48] M. Sabo, A. Henschel, H. Fröde, E. Klemm, S. Kaskel, *J. Mater. Chem.* **2007**, *17*, 3827.
[49] M. Thommes, K. Kaneko, A. V. Neimark, J. P. Olivier, F. Rodriguez-Reinoso, J. Rouquerol, K. S. W. Sing, *Pure Appl. Chem.* **2015**, *87*, 1051.
[50] J. Ren, M. Ledwaba, N. M. Musyoka, H. W. Langmi, M. Mathe, S. Liao, W. Pang, *Coord. Chem. Rev.* **2017**, *349*, 169.
[51] J. Hafizovic, M. Bjørgen, U. Olsbye, P. D. C. Dietzel, S. Bordiga, C. Prestipino, C. Lamberti, K. P. Lillerud, *J. Am. Chem. Soc.* **2007**, *129*, 3612.
[52] A. H. Farmahini, K. Limbada, L. Sarkisov, *Adsorption* **2022**, *28*, 219.
[53] M. D. Ward, P. R. Raithby, *Chem. Soc. Rev.* **2013**, *42*, 1619.
[54] M. Haase, C. G. Hübner, F. Nolde, K. Müllen, T. Basché, *Phys. Chem. Chem. Phys.* **2011**, *13*, 1776.
[55] H. Li, O. S. Wenger, *Angew. Chem., Int. Ed.* **2022**, *61*, 202110491.
[56] D. J. Tranchemontagne, J. R. Hunt, O. M. Yaghi, *Tetrahedron* **2008**, *64*, 8553.
[57] A. Knebel, L. Sundermann, A. Mohmeyer, I. Strauß, S. Friebe, P. Behrens, J. Caro, *Chem. Mater.* **2017**, *29*, 3111.
[58] B. Hourahine, B. Aradi, V. Blum, F. Bonafé, A. Buccheri, C. Camacho, C. Cevallos, M. Y. Deshaye, T. Dumitric, A. Dominguez, S. Ehlert, M. Elstner, T. Van Der Heide, J. Hermann, S. Irle, J. J. Kranz, C. Köhler, T. Kowalczyk, T. Kubař, I. S. Lee, V. Lutsker, R. J. Maurer, S. K. Min, I. Mitchell, C. Negre, T. A. Niehaus, A. M. N. Niklasson, A. J. Page, A. Pecchia, G. Penazzi, et al., *J. Chem. Phys.* **2020**, *152*, 124101.
[59] M. Gaus, A. Goez, M. Elstner, *J. Chem. Theory Comput.* **2013**, *9*, 338.
[60] X. Lu, M. Gaus, M. Elstner, Q. Cui, *J. Phys. Chem. B* **2015**, *119*, 1062.
[61] P. Goyal, H. J. Qian, S. Irle, X. Lu, D. Roston, T. Mori, M. Elstner, Q. Cui, *J. Phys. Chem. B* **2014**, *118*, 11007.
[62] S. Grimme, J. Antony, S. Ehrlich, H. Krieg, *J. Chem. Phys.* **2010**, *132*, 154104.
[63] N. Prasetyo, T. S. Hofer, *Comput. Mater. Sci.* **2019**, *164*, 195.
[64] B. M. Rode, T. S. Hofer, B. R. Randolf, C. F. Schwenk, D. Xenides, V. Vchirawongkwin, *Theor. Chem. Acc.* **2006**, *115*, 77.
[65] B. M. Kriesche, L. E. Kronenberg, F. R. S. Purtscher, T. S. Hofer, *Front. Chem.* **2023**, *11*, 141.
[66] W. C. Swope, H. C. Andersen, P. H. Berens, K. R. Wilson, *J. Chem. Phys.* **1982**, *76*, 637.
[67] H. C. Andersen, *J. Comput. Phys.* **1983**, *52*, 24.
[68] G. Bussi, D. Donadio, M. Parrinello, *J. Chem. Phys.* **2007**, *126*, 14101.
[69] H. J. C. Berendsen, J. P. M. Postma, W. F. Van Gunsteren, A. Dinola, J. R. Haak, *J. Chem. Phys.* **1984**, *81*, 3684.
[70] W. Humphrey, A. Dalke, K. Schulten, *J. Mol. Graph.* **1996**, *14*, 33.